J Neurophysiol 119: 177–191, 2018.
First published October 4, 2017; doi:10.1152/jn.00146.2017.

RESEARCH ARTICLE | *Neural Circuits*

Layer- and subregion-specific differences in the neurophysiological properties of rat medial prefrontal cortex pyramidal neurons

Chenghui Song[1] and James R. Moyer, Jr.[1,2]
[1]*Department of Psychology, University of Wisconsin-Milwaukee, Milwaukee, Wisconsin; and* [2]*Department of Biological Sciences, University of Wisconsin-Milwaukee, Milwaukee, Wisconsin*

Submitted 27 February 2017; accepted in final form 2 October 2017

Song C, Moyer JR Jr. Layer- and subregion-specific differences in the neurophysiological properties of rat medial prefrontal cortex pyramidal neurons. *J Neurophysiol* 119: 177–191, 2018. First published October 4, 2017; doi:10.1152/jn.00146.2017.—Medial prefrontal cortex (mPFC) is critical for the expression of long-term conditioned fear. However, the neural circuits involving fear memory acquisition and retrieval are still unclear. Two subregions within mPFC that have received a lot of attention are the prelimbic (PL) and infralimbic (IL) cortices (e.g., Santini E, Quirk GJ, Porter JT. *J Neurosci* 28: 4028–4036, 2008; Song C, Ehlers VL, Moyer JR Jr. *J Neurosci* 35: 13511–13524, 2015). Interestingly, PL and IL may play distinct roles during fear memory acquisition and retrieval but the underlying mechanism is poorly understood. One possibility is that the intrinsic membrane properties differ between these subregions. Thus, the current study was carried out to characterize the basic membrane properties of mPFC neurons in different layers and subregions. We found that pyramidal neurons in L2/3 were more hyperpolarized and less excitable than in L5. This was observed in both IL and PL and was associated with an enhanced *h*-current in L5 neurons. Within L2/3, IL neurons were more excitable than those in PL, which may be due to a lower spike threshold and higher input resistance in IL neurons. Within L5, the intrinsic excitability was comparable between neurons obtained in IL and PL. Thus, the heterogeneity in physiological properties of mPFC neurons may underlie the observed subregion-specific contribution of mPFC in cognitive function and emotional control, such as fear memory expression.

NEW & NOTEWORTHY This is the first study to demonstrate that medial prefrontal cortical (mPFC) neurons are heterogeneous in both a layer- and a subregion-specific manner. Specifically, L5 neurons are more depolarized and more excitable than those neurons in L2/3, which is likely due to variations in *h*-current. Also, infralimbic neurons are more excitable than those of prelimbic neurons in layer 2/3, which may be due to differences in certain intrinsic properties, including input resistance and spike threshold.

infralimbic; prelimbic; layer 2/3; layer 5; brain slice

INTRODUCTION

The medial prefrontal cortex (mPFC) is critical for both emotional and cognitive processes (e.g., Arruda-Carvalho and Clem 2014; Hayton et al. 2011; Heidbreder and Groenewegen 2003; Varela et al. 2012). Within mPFC, the prelimbic (PL) and infralimbic (IL) subregions play distinct roles in fear learning such that PL activation facilitates the expression of conditioned fear (Burgos-Robles et al. 2009; Vidal-Gonzalez et al. 2006) whereas IL activation reduces conditioned fear and facilitates extinction (Burgos-Robles et al. 2007; Chang and Maren 2011; Milad and Quirk 2002; Milad et al. 2004; Santini et al. 2008; Sepulveda-Orengo et al. 2013; Soler-Cedeño et al. 2016; Vidal-Gonzalez et al. 2006). However, the previous reports are not all consistent, which obscures our understanding of the neural basis underlying fear memory regulation (for review, see Kim and Jung 2006). For example, some earlier studies suggest that fear conditioning suppresses PL neuronal activity (Garcia et al. 1999) and that PL lesions enhance conditioned fear (Morgan and LeDoux 1995). Consistent with these observations, a recent study demonstrated that blockade of NMDA receptors in IL suppresses conditioned fear (Kwapis et al. 2015). Similarly, data from another study suggest that trace fear conditioning inhibits the intrinsic excitability of PL-to-amygdala projection neurons but enhances the excitability of IL-to-amygdala projection neurons (Song et al. 2015). The neurobiological mechanisms underlying such subregion-specific processing of information within mPFC are not clear.

One possible mechanism of the subregion-specific contribution of mPFC to fear memory expression is the differential intrinsic excitability of the neurons within IL and PL. For example, a previous study of layer 2/3 (L2/3) neurons suggests that in adult rats IL neurons are more excitable than PL neurons, and that the subsequent loss of this differential intrinsic excitability during aging may be responsible for the poor extinction memory in middle-aged and aged rats (Kaczorowski et al. 2012). Furthermore, the electrophysiological properties of mPFC neurons are also different across layers, with neurons in L2/3 being more hyperpolarized than those in L5 (Boudewijns et al. 2013). However, most studies do not distinguish between neurons located in different layers and/or subregions, which may contribute to disparate and even apparently controversial results. The present study evaluated the electrophysiological properties of mPFC neurons as a function of both laminar location (L2/3 vs. L5) and subregion (IL vs. PL). The data demonstrate that mPFC neurons display distinct electrophysiological properties in a layer- and subregion-specific manner. Furthermore, the current data suggest that the dendritic morphology, the expression level of hyperpolarization-

Address for reprint requests and other correspondence: J. R. Moyer, Jr., Department of Psychology, P.O. Box 413, University of Wisconsin-Milwaukee, Milwaukee, WI 53201 (e-mail: jrmoyer@uwm.edu).

activated cyclic nucleotide-gated (HCN) channels, as well as input resistance may contribute to these differences.

METHODS

Subjects

Subjects were 11 adult male Sprague-Dawley (4.9 ± 0.9 mo) and 19 adult male Fischer F344 rats (4.7 ± 0.2 mo). Data were combined because no significant differences were observed in all measurements. Rats were maintained in an Association for Assessment and Accreditation of Laboratory Animal Care-accredited facility on a 14-h light–10-h dark cycle and housed individually with free access to food and water. All procedures were conducted according to NIH guidelines under a protocol approved by the University of Wisconsin-Milwaukee animal care and use committee.

Retrobeads Injection

A subset of Fischer F344 rats (3 mo; $n = 4$) received unilateral pressure infusion of a fluorescent retrograde tracer (red Retrobeads, Lumafluor) into the amygdala as described previously (Song et al. 2015). Briefly, the rats received stereotaxic surgery with deep anesthetization, and a glass pipette (tip diameter 20–30 μm) targeting basolateral (BL) nucleus of the amygdala (relative to bregma, −3 mm anteroposterior, ± 5 mm mediolateral; −8.3 mm dorsoventral) was used for Retrobeads infusion. A total of 0.1–0.3 μl red Retrobeads were infused into the basolateral complex of amygdala (BLA).

Slice Preparation and Internal Solutions for Electrophysiological Recording

Rats were anesthetized with isoflurane and decapitated. The brains were then quickly removed and placed in ice-cold oxygenated (95% O_2-5% CO_2) artificial cerebrospinal fluid (aCSF; composition in mM: 124 NaCl, 2.8 KCl, 1.25 NaH_2PO_4, 2 $MgSO_4$, 2 $CaCl_2$, 26 $NaHCO_3$, and 20 dextrose, pH 7.4). The brains were then blocked and coronal prefrontal brain slices (300 μm) were cut in ice-cold aCSF using a vibrating tissue slicer (VT1200, Leica). Slices were transferred to a holding chamber (Moyer and Brown 2007) containing oxygenated aCSF at 32–36°C. Isoflurane has been found to inhibit the neuronal excitability in some brain areas through modulating resting membrane potential (RMP), input resistance, and T-type calcium current. However, these effects are reversible and can be washed out (Becker et al. 2012; Eckle et al. 2012; Joksovic and Todorovic 2010). Thus, it is unlikely that any of our experimental results are due to the anesthetic used during slice preparation, as all slices were incubated for at least 45 min in the holding chamber and perfused for at least 10 min in recording chamber before recording.

For whole-cell recordings (WCRs), electrodes (5–7 MΩ) were prepared from thin-walled capillary glass and filled with the following solution (in mM): 110 K-gluconate, 20 KCl, 10 phosphocreatine di(tris) salt, 10 HEPES, 2 $MgCl_2$, 2 Na_2ATP, 0.3 Na_2GTP, 0.2% biocytin, pH to 7.3. Unless otherwise stated, chemicals were obtained from Sigma or Fisher.

Electrophysiological Recordings

Prefrontal cortical slices were transferred to a submerged recording chamber mounted on an Olympus BX51WI upright microscope where they were continuously perfused with oxygenated aCSF at a rate of 2 ml/min, maintained at 32–36°C using an inline temperature controller. Neurons were visualized with infrared differential video interference microscopy. Somatic WCRs were obtained from 125 regular spiking pyramidal neurons located in either the IL or PL subregions of mPFC (see Fig. 1*A*; Paxinos and Watson 1998). Pyramidal neurons were recognized by their large somata, prominent apical dendrite, and the firing properties. The cell identity was further verified by biocytin staining (see detail in *Visualization and Morphological Analysis of mPFC Neurons* below). The laminar location of each neuron was determined from online image snapshots (Fig. 1*A*) and drawn on the corresponding plates of the rat atlas (Paxinos and Watson 1998). The boundary between L2/3 and L5 was defined according to the somatic depth such that any neuron located within 400 μm of the pial surface was classified as a L2/3 neuron (Gabbott and Bacon 1996; Perez-Cruz et al. 2007). L6 was easily recognized by its high density of fibers (Gaillard and Sauve 1995). Only neurons with an RMP more negative than −50 mV, an input resistance (R_N) > 50 MΩ, an action potential (AP) amplitude > 45 mV relative to threshold, and an access resistance (Rs) less than 40 MΩ were included. Recordings were performed in current-clamp mode using a HEKA amplifier (HEKA Elektronik). For all experiments, neurons were held at −67 mV by manually adjusting the holding current; however, a subset of neurons ($n = 4$) were recorded at both −67 mV and their RMP. The electrode capacitance and Rs were monitored and compensated frequently throughout the duration of the recording. Membrane potentials were not corrected for the liquid junction potential (approximately +13 mV; see Moyer and Brown 2007). In some experiments, HCN channels were blocked by bath application of 50 μM 4-ethylphenylamino-1,2-dimethyl-6-methylaminopyrimidinium chloride (ZD7288; Tocris Bioscience, Ellisville, MO). In addition, before terminating any recording, a photomicrograph of the slice showing the location of the recording electrode in the brain slice was taken with the CCD camera for offline verification of the somatic location (IL vs. PL) and measurement of the somatic depth from the pial surface (see Figs. 1 and 2).

Stimulation and Recording Protocols

Intrinsic properties of mPFC neurons were recorded under current clamp according to the following protocols: *1*) voltage (*V*)-current (*I*) relations were obtained from a series of 500-ms current injections (range −300 to 50 pA) and plotting the plateau voltage deflection against current amplitude. Neuronal input resistance (R_N) was determined from the slope of the linear fit of the portion of the *V-I* plot (Fig. 3*A*) where the voltage sweeps did not exhibit sags or active conductance. The depolarizing sag was calculated from the voltage response to −200 pA, −250 pA, and −300 pA hyperpolarization currents and averaged (Fig. 3*A*). The sag ratio during hyperpolarizing membrane responses was expressed as $[(1–\Delta V_{ss} / \Delta V_{max}) \times 100\%]$, where $\Delta V_{ss} = MP–V_{ss}$, $\Delta V_{max} = MP - V_{max}$; MP is the membrane potential before current step; V_{ss} is the steady-state potential at the end of the current step; V_{max} is the peak amplitude during the first 150 ms of the current step. *2*) AP properties, including $I_{threshold}$ (the minimum current necessary to elicit an AP), were studied with an ascending series of 500 ms depolarizing pulses to elicit one single spike (regular spikers, Fig. 4*A*). Neurons that fired more than one AP in response to the $I_{threshold}$ were defined as bursting cells (Connors et al. 1982; Moyer et al. 2002) and were not further analyzed due to their relatively low numbers (5 of 113 neurons). AP threshold was defined as the voltage when d*V*/d*t* first exceeded 28 mV/ms (Kaczorowski et al. 2012). The AP amplitude was measured relative to the AP threshold. Fast afterhyperpolarization (fAHP) was defined as the negative going peak relative to AP threshold within 2–5 ms. (Fig. 4*A*). AP width was measured as the width at half of the AP amplitude. *3*) Neuronal excitability was assessed by counting the number of spikes evoked in response to a series of 1-s depolarizing steps (range 50–300 pA, at 50 pA increments; 20 s intertrial interval, see Fig. 5, *A* and *C*). *4*) The postburst afterhyperpolarization (AHP) was studied following a 50-Hz burst of 10 spikes, each of which were evoked by a 2-ms suprathreshold current injection (3×, at 20-s intervals). The amplitude of the AHP was measured at different time points following the offset of the last current injection (Fig. 5, *B* and *D*).

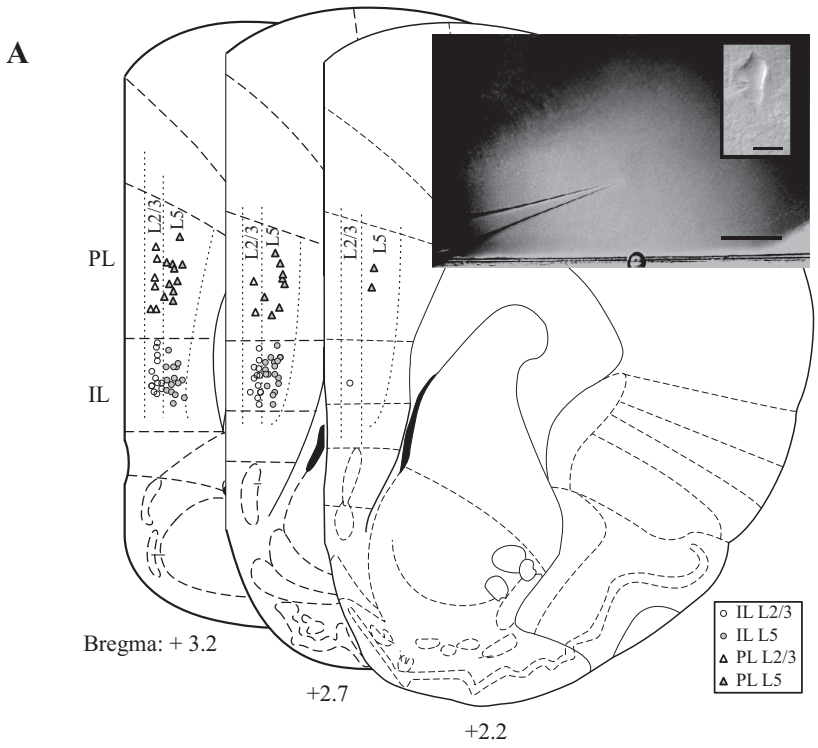

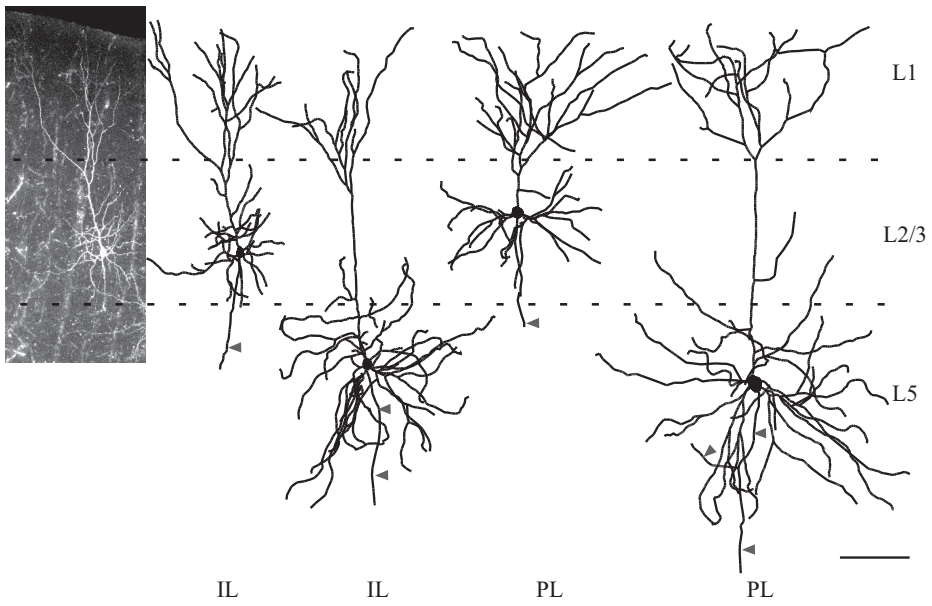

Fig. 1. Distribution of recordings within medial prefrontal cortex (mPFC). *A*: location of each recorded neuron was obtained from a photomicrograph taken after each experiment and indicated as individual symbol in brain stereotaxic atlases (Paxinos and Watson 1998). *Inset*, representative low-power image of patch pipette in prelimbic L5 (scale bar 500 μm) along with a high-power image of an infrared-differential interference contrast image of a neuron recorded from prelimbic L5 (scale bar 10 μm). *B*: representative confocal image shows a neuron recorded from infralimbic (IL) L2/3 (*left*) along with 3D reconstructions of this and 3 other neurons in different layers of IL and prelimbic (PL). Arrowheads point to axons. Scale bar, 100 μm.

To study synaptically evoked excitatory postsynaptic potentials (EPSPs) in IL-BLA projection neurons, parallel stimulating electrodes with polytetrafluoroethylene-coated platinum-iridium wires in glass pipettes (a tip size of $<$60 μm) were custom made in the laboratory. The small-diameter tip allowed for the placement of two stimulating electrodes within a small space. Layer 5 IL-BLA projection neurons were visualized using an Olympus microscope (BX51WI) equipped with mercury lamp and a Texas Red epifluorescent filter cube. A Hamamatsu CCD camera (Hamamatsu Camera, Tokyo, Japan) was used to visualize neurons. After fluorescently labeled projection neurons were identified, the microscope was switched to infrared differential interference contrast mode to guide establishment of WCRs. The synaptic properties of IL-BLA projection neurons were studied according to the following protocol: *1*) Single EPSPs were evoked by stimulating L2/3 pathway (Fig. 7*A*). *2*) Temporal summation was studied by stimulating the L2/3 pathway to elicit a train of EPSPs at 20, 50, and 100 Hz. *3*) Signal integration (coincidence detection) was studied by stimulating both L2/3 and L5 inputs and varying the delay between the two stimuli (Fig. 7*D*). Stimulation intensity for each electrode was adjusted so that the postsynaptic neuron only fired an AP when both stimulation pathways were activated simultaneously.

Visualization and Morphological Analysis of mPFC Neurons

Biocytin-filled neurons were fixed in formalin for 1 to 2 wk and processed for visualization using a streptavidin Alexa Fluor 488

reaction as previously described (Song et al. 2012). Briefly, the slices were incubated in 3% H_2O_2-10% methanol for 45 min, washed with PBS, followed by 0.4% Triton X-100/2% BSA for 45 min. The slices were then incubated with 1:500 streptavidin Alexa Fluor 488 (Invitrogen/Life Technologies) for 2 h in the dark, and washed with PBS. They were mounted onto slides, coverslipped with Ultra Cruz Mounting Medium (Santa Cruz Biotechnology, Santa Cruz, CA), and sealed with nail polish.

The labeled neurons were visualized and imaged using a laser scanning confocal fluorescence microscope and appropriate filter sets (FV-1200, Olympus). Confocal *z*-stacks were taken from neurons with intact and bright apical and basal dendrites for further analysis of dendritic morphology. The stacks of images were taken by using either a ×10 or a ×20 objective (numerical aperture 0.4 and 0.75, respectively) with voxel dimensions of 0.62 × 0.62 × 0.62 μm. The images were imported into Neurolucida software (MBF Bioscience) and reconstructed in 3D (see representative images in Fig. 1*B*). Neuron reconstruction data were imported into NeuroExplorer (MBF Bioscience) for assessment of dendritic length and complexity (number of intersections and bifurcation nodes), and the 3D convex hull (CH) volume (i.e., the volume encompassing all projection end points) was determined for both apical and basal dendrites.

Statistical Analyses

All statistical analyses were performed using IBM SPSS statistics software (version 22; SPSS). Initially, a Shapiro-Wilk normality test was used to assess whether the data conformed to a normal distribution. Nonparametric tests (independent-samples Kruskal-Wallis test with post hoc Mann-Whitney *U*-tests or Spearman correlation analysis) were used when the Shapiro-Wilk normality test was low ($P \leq 0.05$), otherwise appropriate parametric tests (two-tailed independent samples *t*-test, paired *t*-test, one-way ANOVA with post hoc Fisher LSD test, Pearson correlation analysis, or a repeated-measures ANOVA with post hoc Fisher LSD test) were used. *P* values were reported either as actual numbers or as <0.001. All results were reported as means ± SE.

RESULTS

Basic Membrane Properties of mPFC Neurons Vary as a Function of Layer and Subregion

Numerous factors contribute to and modulate intrinsic excitability, including RMP (O'Leary et al. 2010), input resistance (Aou et al. 1992), depolarizing sag (Fan et al. 2005), and AP threshold (Daoudal and Debanne 2003). Thus, these basic membrane properties were characterized in all recordings from mPFC neurons.

Resting membrane potential. One-way ANOVA revealed that the RMP was significantly different as a function of layer [$F(3,121) = 15.5$, $P < 0.001$]. Neurons obtained from L2/3 had an RMP that was significantly more negative compared with those obtained from L5 (see Table 1). Furthermore, there was a significantly positive correlation between the RMP and the somatic depth such that neurons in superficial layers had more negative RMPs than neurons in deep layers (see Fig. 2; $P < 0.001$ for neurons in both IL and PL, Pearson's correlations). Thus, unless otherwise noted, all experiments were carried out at a membrane potential of −67 mV under current-clamp conditions. The average holding current was positive in L2/3 neurons and negative in L5 neurons and they were significantly different in both IL and PL [see Table 1. $F(3, 115) = 13.3$, $P < 0.001$, one-way ANOVA followed Fisher's LSD post hoc test].

Input resistance. The input resistance was significantly different between neurons from IL and PL. As shown in Fig. 3*B* and Table 1, in both L2/3 and L5, IL neurons had significantly larger input resistance than that of PL neurons [independent samples Kruskal-Wallis test ($\chi^2_{3,125} = 14.9$, $P = 0.002$) with Mann-Whitney *U*-test ($t = 2.5$, $P = 0.012$ for L2/3 and $t = 2.2$, $P = 0.025$ for L5, respectively)]. The input resistance was not significantly different between layers within the same subregion, in either IL or PL ($P = 0.23$ for IL and $P = 0.07$ for PL, respectively).

Depolarizing sag. In response to hyperpolarizing current injections, the membrane voltage of mPFC neurons showed depolarizing sags that were characteristic of *h* current (I_h) activation (Fig. 3*A*). Cells in deep layer (L5) displayed larger depolarizing sags than those in superficial layers (L2/3) in both IL and PL [Table 1 and Fig. 3*B*; independent samples Kruskal-Wallis test ($\chi^2_{3,109} = 34.7$, $P < 0.001$) with Mann-Whitney *U*-test ($t = 3.7$, $P = 0.001$ for IL and $t = 4.6$, $P = 0.001$ for PL). In addition, there was a significantly positive correlation between the sag ratio and the somatic depth (see Fig. 3*C*; $P < 0.01$ in both IL and PL; Spearman correlations), suggesting that more HCN channels are expressed in neurons in the deep layers than those in the superficial layers.

Action potential threshold. As shown in Table 2 and Fig. 4*B*, spike threshold was significantly lower in infralimbic L2/3

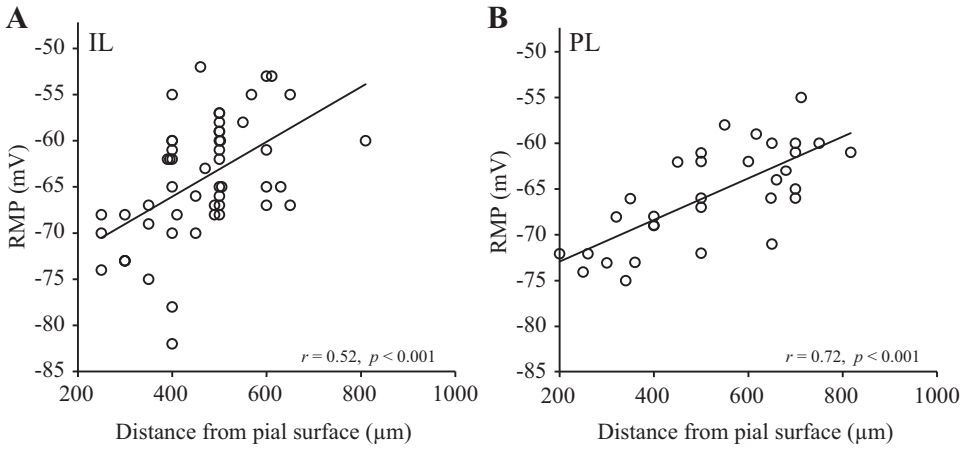

Fig. 2. Within mPFC, RMP is significantly correlated with somatic depth. *A*: plot of RMP vs. somatic depth in IL ($n = 53$). *B*: plot of RMP vs. somatic depth in PL ($n = 32$). Somatic depth was measured as the distance of the soma from the pial surface. RMP was measured as the membrane potential when whole-cell recording was obtained (*r*, Pearson's coefficient).

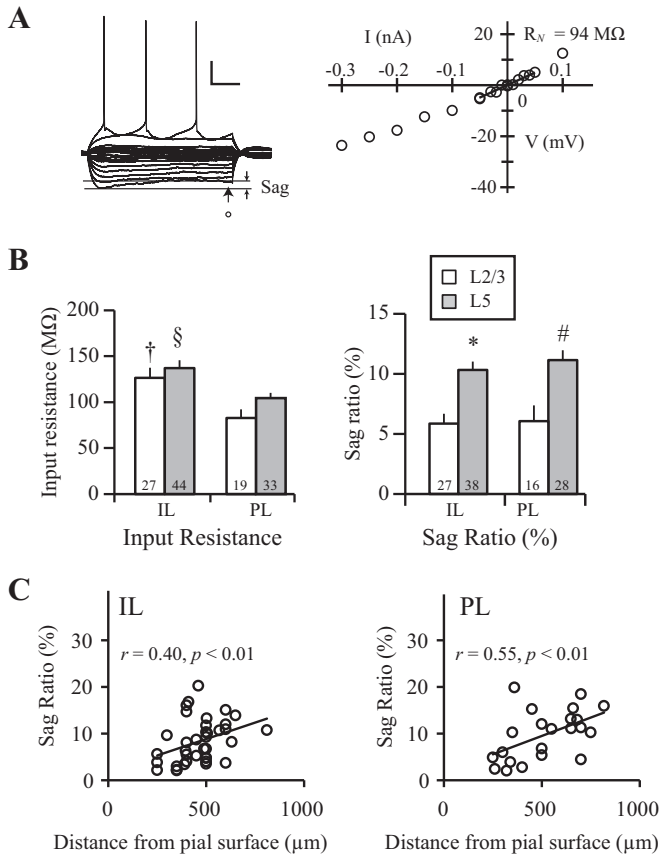

Fig. 3. Basic membrane properties of mPFC neurons are layer and subregion specific. *A*: representative voltage sweeps (*left*) used to generate the voltage (*V*)-current (*I*) plot (*right*). Input resistance was calculated from the slope of the linear fit of the steady-state voltage responses generated in response to small hyperpolarizing and depolarizing current injections. Thick arrow indicates the location where steady-state voltage response was measured. The sag ratio was calculated from the depolarizing sag (between the thin arrows) in response to hyperpolarization (see METHODS). Scale bar, 20 mV, 100 ms. *B*: bar graphs (mean ± SE) showing different membrane properties between layers and subregions. Numbers located within the bar graphs represent the number of cells in that group. *Left*, IL neurons had a significantly higher input resistance than PL neurons in both L2/3 and L5 [†IL L2/3 was statistically different from PL L2/3 ($P = 0.012$); §IL L5 was statistically different from PL L2/3 ($P < 0.001$) and PL L5 ($P = 0.025$)]. *Right*, L5 neurons had a significantly larger sag ratio than that of L2/3 neurons [*IL L5 was statistically different from IL L2/3 ($P < 0.001$) and PL L2/3 ($P < 0.001$); #PL L5 was statistically different from IL L2/3 ($P < 0.001$) and PL L2/3 ($P < 0.001$)]. *C*: sag ratio is significantly correlated with somatic depth in both IL ($n = 48$) and PL ($n = 29$; *r*, Pearson's coefficient).

neurons compared with those in infralimbic L5 and prelimbic L5 neurons [independent samples Kruskal-Wallis test ($\chi^2_{3,113} = 12.6$, $P = 0.006$) with Mann-Whitney *U*-test ($t = 3.4$, $P = 0.001$ for IL L5 and $t = 2.6$, $P = 0.01$ for PL L5, respectively]. In contrast, spike threshold did not vary as a function of layer within PL ($t = 0.83$, $P = 0.41$; Mann-Whitney *U*-test). However, within PL there was a layer-specific difference in $I_{threshold}$ (the minimum current necessary to evoke an AP) such that $I_{threshold}$ was significantly greater in neurons obtained from prelimbic L2/3 than in neurons obtained from prelimbic L5, infralimbic L2/3, and infralimbic L5 [independent samples Kruskal-Wallis test ($\chi^2_{3,113} = 13.6$, $P = 0.003$) with Mann-Whitney *U*-test ($t = 3.4$, $P = 0.001$ for PL L5; $t = 2.7$, $P = 0.008$ for IL L2/3; $t = 3.4$, $P = 0.001$ for IL L5)], suggesting that prelimbic L2/3 neurons are less excitable than prelimbic L5, infralimbic L2/3, and infralimbic L5 neurons. No significant differences were observed when comparing between different layers or subregions for other properties such as AP amplitude, AP width, and fAHP.

Intrinsic Excitability of mPFC Neurons Varies in a Layer- and Subregion-Specific Manner

The intrinsic excitability of mPFC neurons was evaluated by counting the number of spikes evoked by a series of depolarizing current steps (see a representative trace in Fig. 5*A* and averaged data in Fig. 5*C*). A two-way repeated-measures ANOVA revealed a significant main effect of subregion [$F(3, 107) = 3.4$, $P = 0.019$] and current intensity [$F(1.3, 140) = 215$, $P < 0.001$; Greenhouse-Geisser corrected] with a significant subregion × current intensity interaction [$F(3.9, 140) = 2.9$, $P = 0.026$]. Fisher's LSD post hoc test revealed that prelimbic L2/3 neurons fired significantly fewer APs than did prelimbic L5 ($P = 0.020$), infralimbic L5 ($P = 0.005$), and infralimbic L2/3 ($P = 0.005$) neurons (see Fig. 5*C* and Table 3). No significant differences in excitability between L2/3 and L5 neurons were observed within IL ($P = 0.91$). It is possible any differences in excitability between L2/3 and L5 neurons within IL were obscured by our use of a consistent holding potential of −67 mV for all experiments. To test this hypothesis, the excitability within IL was evaluated from a subset of L2/3 neurons ($n = 5$) at both rest (−75 ± 1.6 mV) and a −67 mV holding potential. As shown in Fig. 5*E*, the excitability of these neurons was significantly lower at rest relative to when they were depolarized to −67 mV [$F(1,8) = 23.4$, $P = 0.01$, repeated-measures ANOVA, followed by paired *t*-test; $*P < 0.05$]. Thus, these results suggest that L2/3 neurons are generally less excitable than L5 neurons in both IL and PL at their RMP.

The postburst AHP is another index of intrinsic excitability. A repeated-measures ANOVA revealed that the size of the postburst AHP also varied as a function of neuronal location [$F(3,107) = 3.5$, $P < 0.02$], such that the AHP was significantly smaller in prelimbic L2/3 neurons than that of prelimbic L5 ($P = 0.002$), infralimbic L5 ($P = 0.025$), and infralimbic L2/3 neurons ($P = 0.016$; see Fig. 5*D*; one-way ANOVA with Fisher's LSD post hoc test). As can be seen in Table 3 and Fig. 5*D*, the post hoc analysis revealed that within IL AHP amplitude did not vary as a function of layer ($P = 0.7$). This lack of a difference in postburst AHP between L2/3 and L5 neurons within IL may have been obscured by the use of a consistent holding potential of −67 mV. To evaluate this possibility, the postburst AHP was measured in a subset of neurons at both rest and at −67 mV. As shown in Fig. 5*F*, the postburst AHP was significantly smaller when studied at their more hyperpolarized resting potential than at −67 mV [$F(1,8) = 23.8$, $P = 0.001$, repeated-measures ANOVA, followed by paired *t*-test; $\#P < 0.01$; $*P < 0.05$]. These results suggest that mPFC pyramidal neurons located in the more superficial L2/3 have significantly smaller AHPs than their deeper counterparts in L5.

Dendritic Arborization Is Correlated with Intrinsic Excitability

Analysis with 3D reconstruction of recorded neurons suggested that the CH volume and complexity of basal dendrites significantly affected membrane properties and intrinsic excit-

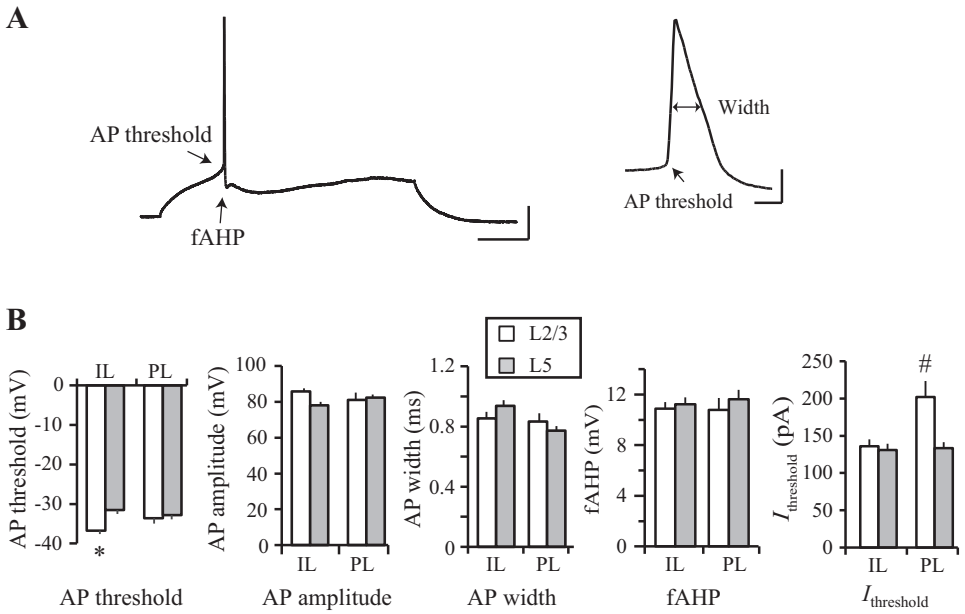

Fig. 4. Layer- and subregion-specific differences in action potential characteristics of mPFC neurons. *A*: representative traces of a single action potential (AP) evoked by a threshold current ($I_{threshold}$). AP threshold was defined as the voltage when d*V*/d*t* first exceeded 28 mV/ms. AP amplitude was measured from threshold. Fast afterhyperpolarization (fAHP) was defined as the different potential between the AP threshold and the initial negativity that followed the repolarization of the AP. AP width was measured as the width at half of the AP amplitude (from threshold). Scale bar, 100 ms, 20 mV (*left*); 1 ms, 20 mV (*right*). *B*: bar graphs (mean ± SE) showing the AP characteristics of mPFC neurons from 28 infralimbic L2/3 neurons, 17 prelimbic L2/3 neurons, 37 infralimbic L5 neurons, and 31 prelimbic L5 neurons. Infralimbic L2/3 neurons had a significantly lower AP threshold, whereas prelimbic L2/3 neurons had a significantly higher $I_{threshold}$ [*AP threshold in IL L2/3 was statistically different from IL L5 ($P = 0.001$) and PL L5 ($P = 0.010$); #$I_{threshold}$ in PL L2/3 was statistically different from IL L2/3 ($P = 0.008$), IL L5 ($P = 0.001$), and PL L5 ($P = 0.001$); one-way ANOVA followed Fisher's LSD post hoc test].

ability. For example, the volume of basal but not apical dendrite was significantly correlated with the sag ratio (see Table 4). Furthermore, there were significant correlations between number of spikes evoked by depolarizing currents and total number of nodes, segments, and ends (see Table 4). Only one apical dendrite measurement (the volume) was found to be significantly correlated with input resistance (Table 4). Taken together, these data suggest that the volume and the complexity of basal dendrites (the number of nodes, segments, and ends) are important factors that affect intrinsic excitability of mPFC neurons.

Blocking HCN Channels Significantly Alters Intrinsic Excitability of L5 Pyramidal Neurons

To test the possible contributions of ion channels that account for the differential excitability in mPFC neurons, we blocked HCN channels by bath applying ZD7288 (50 μM) and investigated the contribution of HCN channels on electrophysiological properties of L5 mPFC neurons. Neurons from IL ($n = 11$) and from PL ($n = 4$) were combined because no significant differences between these two groups of neurons were observed. As shown in Fig. 6, *A–C*, blocking HCN channels dramatically changed the basic membrane properties and AP characteristics including RMP, input resistance, sag ratio, $I_{threshold}$, fAHP, AP threshold, and AP width (for all measurements, $P < 0.01$, paired *t*-test). Furthermore, blocking HCN channels significantly reduced the medium portion of the postburst AHP but slightly enhanced the slow portion [see Fig. 6*D*. $F(1,18) = 10.4$, $P = 0.005$; repeated-measures ANOVA followed by paired *t*-test]. However, no significant effect of HCN channel blockade was observed on L2/3 neurons [see Fig. 6. $F(1,6) = 0.61$, $P = 0.46$; repeated-measures ANOVA], which is consistent with previous studies showing that L2/3 neurons have less I_h and that HCN channels are primarily expressed in L5 neurons (Boudewijns et al. 2013; Lörincz et al. 2002). In addition, blocking HCN channels significantly increased the number of spikes evoked by depolarization when the neurons were held at −67 mV in L5 [see Fig. 6*E*; $F(1,18) = 4.6$, $P = 0.045$; repeated-measures ANOVA followed by paired *t*-test] but not L2/3 neurons [$F(1,6) = 1.45$, $P = 0.27$; repeated-measures ANOVA], perhaps due to the dramatic effects of I_h blockade on the mAHP, input resistance, $I_{threshold}$, and AP threshold (Fig. 6). Thus, these observations suggest that the different expression levels HCN channels account, at least partially for the observed differential membrane properties between L2/3 and L5 neurons.

Blocking HCN Channels Facilitates Signal Integration and Coincidence Detection in L5 Neurons

The layer-specific distribution of HCN channels within mPFC suggest that L2/3 and L5 neurons have different computational properties to process incoming signals. Previous studies in hippocampal neurons suggest that HCN channels are more densely expressed in distal dendrites than proximal dendrites (Magee 1998) and greatly affect temporal summation (Magee 1999), as well as coincidence detection (Pavlov et al. 2011). Even within the same brain region and same layer, cortical neurons that project to different targets may display distinct membrane properties due to their different subtypes and expression levels of HCN channels (Dembrow et al. 2010, 2015). We therefore studied the role of HCN channels on dendritic signal integration in layer 5 IL-BLA neurons, because they are critical for the expression and extinction of conditioned fear (Song et al. 2015). We first studied the effect of

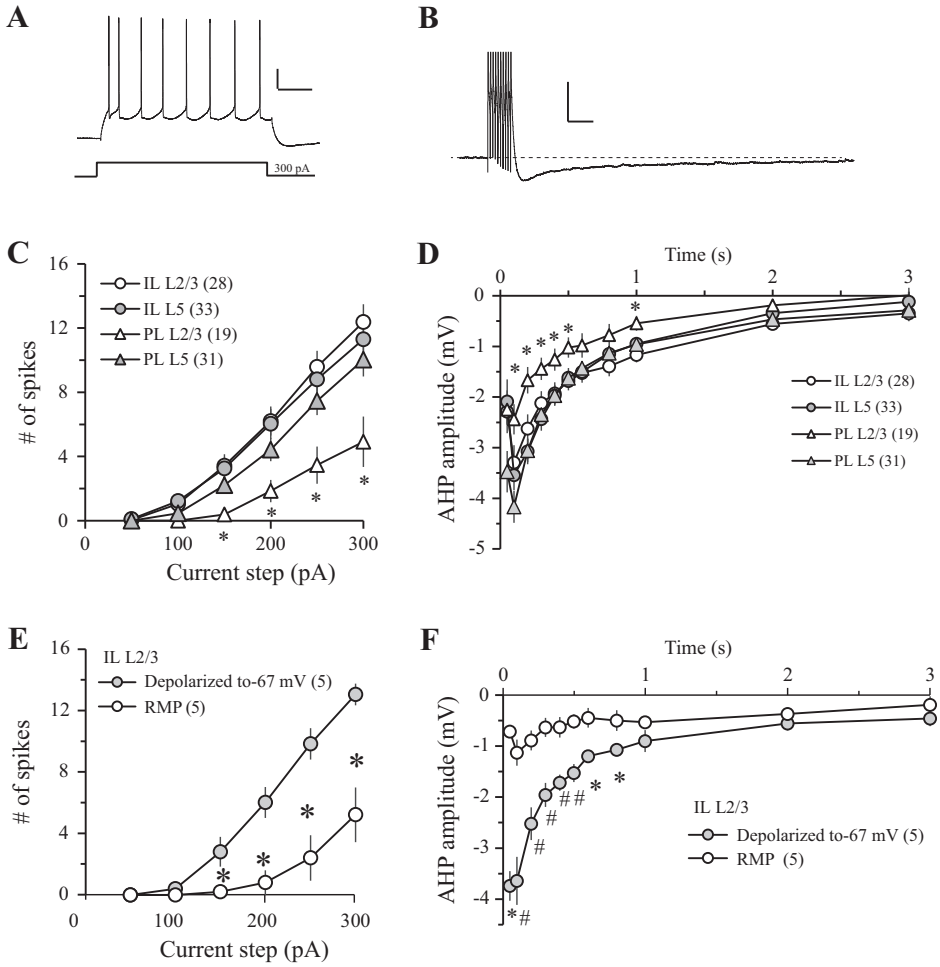

Fig. 5. L2/3 mPFC neurons are less excitable than L5 mPFC neurons. Intrinsic excitability was studied by counting the number of spikes evoked by a series of depolarizing current injections (see a representative trace in *A*; scale bar, 20 mV, 0.2 s). Postburst AHP was measured from multiple time points following a burst of 10 APs evoked by brief current injections at 50 Hz (see a representative trace in *B*; scale bar, 10 mV, 0.2 s). Prelimbic pyramidal neurons obtained in L2/3 showed the least excitability (*C*) and smallest postburst AHP (*D*) compared with prelimbic L5 neurons and infralimbic L2/3 neurons (repeated-measures ANOVA followed by Fisher's LSD test; $*P < 0.05$ between PL L2/3 and all other neurons). Although infralimbic L2/3 neurons displayed comparable excitability and postburst AHP when held at −67 (*C* and *D*), they were significantly less excitable (*E*) and displayed smaller postburst AHP (*F*) at their more hyperpolarized RMP compared with their more depolarized holding potential of −67 mV (repeated-measures ANOVA followed by paired *t*-test; $*P < 0.05$, $\#P < 0.01$; number of cells are in parentheses).

blocking HCN channels on single EPSPs by stimulating fibers in L2/3 while the cells were held at −67 mV (see Fig. 7*A*). As shown in Fig. 7*B*, bath application of 50 μM ZD7288 increased the duration of single EPSPs on the layer 5 IL-BLA projection neurons [$t(7) = 3.8$, $P = 0.007$, paired *t*-test], suggesting that blocking HCN channels increases the time window for signal integration. This was tested by stimulating layer 2/3 inputs and evoking a train of five EPSPs at frequencies of 20, 50, or 100 Hz. As shown in Fig. 7*C*, blocking HCN channels facilitated signal integration, with its maximal effects at the lower frequency stimulation of 20 Hz [$F(1,12) = 9.05$, $P = 0.011$; repeated-measures ANOVA followed by paired *t*-test] but no significant effect at higher frequency stimulation of 50 Hz and 100 Hz [$F(1, 12) = 0.18$, $P = 0.68$ for 50 Hz stimulation and $F(1,12) = 0.35$, $P = 0.57$ for 100 Hz stimulation, respectively; repeated-measures ANOVA]. This suggests that, under normal conditions, *h*-current restricts signal integration at low frequencies but allows integration for high-frequency stimuli.

In contrast to temporal summation that occurred on the same synaptic input, coincidence detection is the process by which the neurons integrate input signals that are temporally close but spatially distributed. We thus examined the effect of ZD7288 on coincidence detection of layer 5 IL-BLA projection neurons by stimulating inputs in L2/3 and L5 to represent two afferent pathways (see Fig. 7*D*). The stimulating intensities were adjusted so that the neurons consistently fired APs only when the two stimulations were delivered simultaneously. We then ob-

Table 1. *Basic membrane properties of mPFC neurons are layer- and subregion-specific*

	Somatic Depth, μm	RMP, mV	I_{hold}, pA	R_N, MΩ	Sag, %
IL					
L2/3	348 ± 11 (26)	−68.8 ± 1.2 (29)	28 ± 18 (27)	122 ± 10 (29)†	6.1 ± 0.7 (27)
L5	534 ± 14 (32)*	−62.2 ± 0.8 (44)*	−54 ± 10 (42)*	134 ± 8 (44) †	10.3 ± 0.7 (38)*
PL					
L2/3	322 ± 16 (17)	−69.5 ± 1.1 (19)	66 ± 27 (19)	85 ± 9 (19)	5.3 ± 1.2 (16)
L5	630 ± 22 (21)*	−63.3 ± 0.7 (33)*	−38 ± 9 (31)*	107 ± 6 (33)	11.2 ± 0.8 (28)*

Data are means ± SE for no. of cells in parentheses. I_{hold}, the current used to hold neurons at −67 mV; IL, infralimbic cortex; PL, prelimbic cortex; R_N, neuronal input resistance; RMP, resting membrane potential. Somatic depth is the distance measured from the soma to the pial surface. *Statistically different between L2/3 and L5, $P < 0.01$; †Statistically different between IL and PL, $P < 0.05$. Statistical analysis was performed using one-way ANOVA followed by Fisher's LSD post hoc test (RMP), or Kruskal-Wallis test followed by Mann-Whitney *U*-test test (somatic depth, I_{hold}, R_N, and Sag).

Table 2. *Action potential characteristics of mPFC neurons*

	AP amplitude, mV	AP width, s	AP threshold, mV	fAHP, mV	$I_{threshold}$, pA
IL					
L2/3	86 ± 2 (28)	0.83 ± 0.04 (27)	−36.6 ± 0.8 (28)*†	10.7 ± 0.5 (28)	141 ± 9 (28)
L5	79 ± 2 (37)	0.91 ± 0.04 (37)	−31.9 ± 0.9 (37)	10.8 ± 0.6 (37)	132 ± 8 (37)
PL					
L2/3	81 ± 3 (17)	0.82 ± 0.05 (17)	−33.9 ± 1.3 (17)	10.2 ± 0.9 (17)	206 ± 20 (17)*‡
L5	82 ± 2 (31)	0.78 ± 0.03 (31)	−32.9 ± 0.9 (31)	11.1 ± 0.7 (31)	131 ± 7 (31)

Data are means ± SE for number of cells in parentheses. IL, infralimbic cortex; PL, prelimbic cortex; AP, action potential; fAHP, fast AHP. *Statistically different between L2/3 and L5, $P < 0.01$; †Statistically different between IL and PL, $P < 0.05$; ‡Statistically different between IL and PL, $P < 0.01$. Statistical analysis was performed using one-way ANOVA followed by Fisher's LSD post hoc test (AP threshold), or Kruskal-Wallis test followed by Bonferroni's post hoc test ($I_{threshold}$).

served the firing activities of the neurons while systematically varying the interstimulus interval (ISI). As shown in Fig. 7*E*, under control conditions, the neuron readily fired APs when the ISI was between 0 and 9 ms. However, after blocking HCN channels, the neuron readily fired APs even when the ISI ranged from −12 to 39 ms. Thus, under physiological conditions, the role of HCN channels is to restrict signal integration so that different afferent information can be integrated only when they occurred within a very short period (i.e., coincidence detection). Blocking HCN channels greatly broadened the time course over which inputs can be integrated within a neuron.

DISCUSSION

The current study provides the first systematic evaluation of laminar- and subregion-specific differences in the electrophysiological properties of mPFC pyramidal neurons. In both IL and PL, neurons obtained in L2/3 were more hyperpolarized and less excitable than those in L5. Such layer-specific properties of mPFC neurons are likely due to differential dendritic architecture and ion channel expression because the RMP was significantly correlated with the somatic depth, and that the cells in deep layers displayed larger I_h current carried by HCN channels. The role of HCN channels was further demonstrated by blocking HCN channels, which dramatically changed the membrane properties of L5 mPFC neurons. Furthermore, several characteristics of mPFC neurons are also subregion specific. For instance, L2/3 neurons located in IL had a higher input resistance and were more excitable than L2/3 neurons within PL. Thus, these data may help to enhance our understanding of the region-specific contributions of mPFC in various cognitive functions, including the processing of emotional information.

Table 3. *Excitability of mPFC neurons*

	Number of Spikes	mAHP, mV	sAHP, mV
IL			
L2/3	11.6 ± 1.0 (28)	−3.9 ± 0.3 (27)	−1.2 ± 0.1 (27)
L5	11.2 ± 1.2 (34)	−4.3 ± 0.3 (39)	−0.9 ± 0.1 (39)
PL			
L2/3	6.1 ± 2.0 (19)*§	−2.8 ± 0.3 (15)†‡	−0.5 ± 0.1 (15)*
L5	10.7 ± 1.1 (31)	−4.9 ± 0.2 (31)	−1.0 ± 0.1 (31)

Data are means ± SE for number of cells in parentheses. IL, infralimbic cortex; PL, prelimbic cortex; mAHP, medium afterhyperpolarization; sAHP, slow afterhyperpolarization. mAHP was measured at the peak of the AHP following a burst of 10 APs relative to baseline. sAHP was measured at 1 s following the offset of the current injection. Number of spikes was counted in response to a 1-s 300-pA depolarizing current injection. *Statistically different between L2/3 and L5, $P < 0.05$; †Statistically different between L2/3 and L5, $P < 0.01$. Statistically different between IL and PL: ‡$P < 0.05$; §$P < 0.01$. Statistical analysis was performed using one-way ANOVA followed by Fisher's LSD post hoc test.

L5 Neurons Are More Excitable Than L2/3 Neurons

Within both IL and PL, neurons obtained from L2/3 were significantly more hyperpolarized than those obtained from L5. This suggests that neurons in superficial layers are less excitable than those in deep layers. This was demonstrated in PL even when all neurons were held at the same membrane potential (−67 mV); neurons from L2/3 fired significantly fewer spikes in response to depolarizing currents (Fig. 5*C*). Within IL, L2/3 neurons were less excitable than L5 neurons when they were recorded at rest (Fig. 5*E*). In addition, L5 neurons had significantly larger depolarizing sags, suggesting higher expression of HCN channels than in L2/3 neurons. Although such layer-specific properties have been reported in visual cortex (Mason and Larkman 1990; Medini 2011) and PL (Boudewijns et al. 2013), the current study is the first to report that these properties are significantly correlated with somatic distance from the pial surface (see Figs. 2 and 3). In addition to the RMP and sag, there are other measurements ($I_{threshold}$, postburst AHP, and no. of spikes evoked by depolarizing current injection) that were significantly correlated with somatic depth, especially in PL, suggesting that these properties gradually change as a function of somatic depth (see Table 5). Thus, understanding such depth-dependent variation of the intrinsic excitability

Table 4. *Correlations between morphology and electrophysiological properties*

Measurements	Apical Dendrite			Basal Dendrite		
	n	*r*	*P*	*n*	*r*	*P*
Dendritic CH volume						
R_N	9	0.68	0.044*	9	−0.02	0.96
Sag	9	0.46	0.21	9	0.68	0.006†
Excitability (no. of spikes)						
No. of nodes	9	0.28	0.47	9	0.68	0.029*
No. of segments	9	0.27	0.48	9	0.69	0.022*
No. of ends	9	0.23	0.55	9	0.71	0.016*

CH volume, convex hull volume; R_N, input resistance; $I_{threshold}$, threshold current required to elicit an action potential. *Significant correlation for Pearson's correlation coefficient, $P < 0.05$; †Significant correlation for Pearson's correlation coefficient, $P < 0.01$.

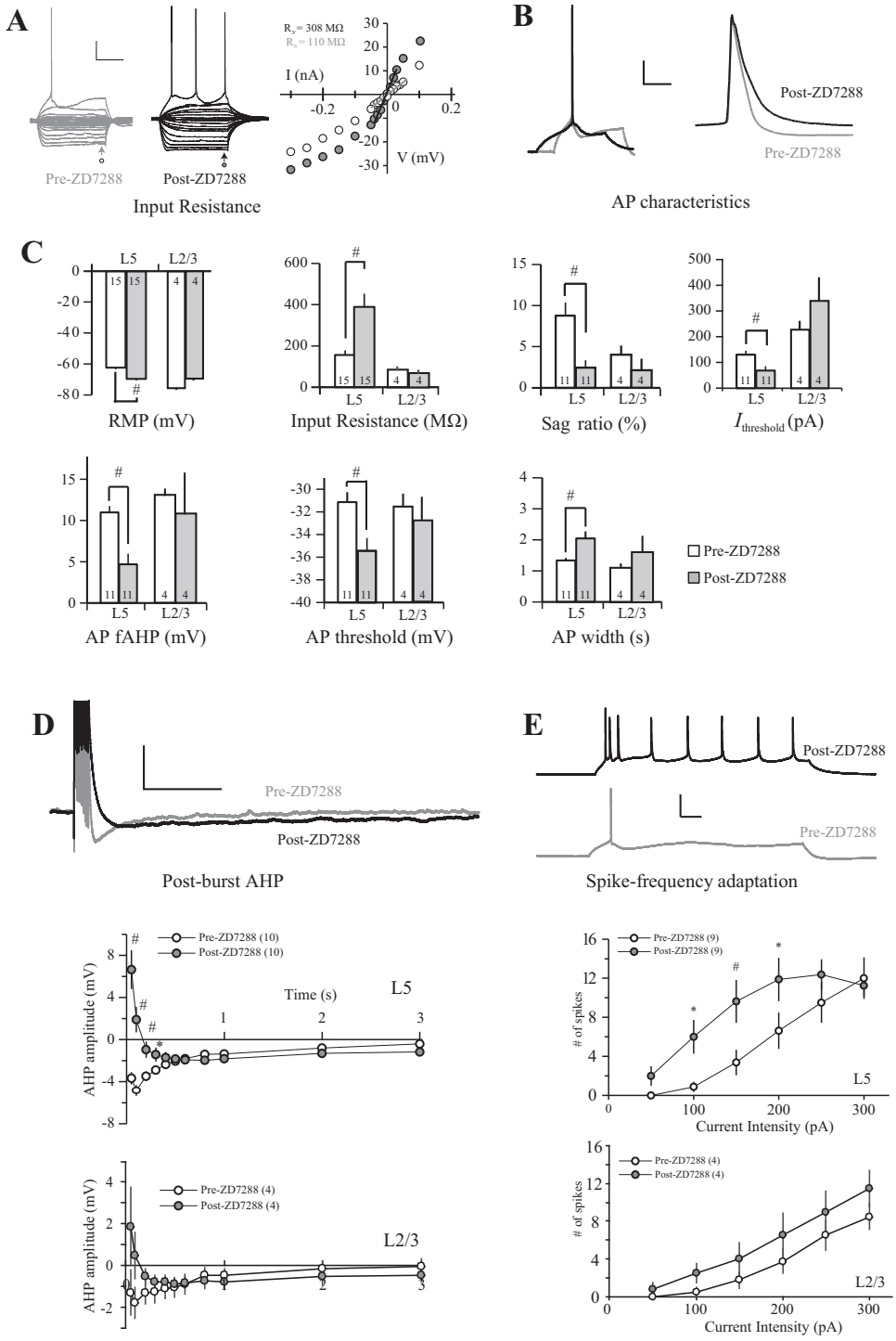

Fig. 6. Blocking hyperpolarization-activated cyclic nucleotide-gated (HCN) channels significantly affects both passive and active membrane properties of L5 mPFC neurons. *A–C*: blocking HCN channels significantly changed passive membrane properties and AP characteristics (bar graphs are means ± SE; numbers located within the bar graphs represent the number of cells in that group; statistically different between pre- and post-application of HCN channel blocker ZD7288: #$P < 0.01$; paired *t*-test). Scale bars: *A*: 20 mV, 200 ms; *B*: 20 mV, 2 ms. *D*: blocking HCN channels diminished the medium AHP (measured between 50–150 ms following the offset of the last current injection) but enhanced the slow AHP (measured ≥800 ms following the offset of the last current injection). *Top*: representative voltage traces; *middle*: plot of average data for L5 neurons; *bottom*: plot of average data for L2/3 neurons. Statistically different between before and after application of HCN channel blocker ZD7288, *$P < 0.05$; #$P <$ 0.01 (repeated-measures ANOVA followed by paired *t*-test). Scale bar: 10 mV, 1 s. *E*: blocking HCN channels enhances neuronal excitability. The neurons fired significantly more spikes in response to depolarizing current injection (*top panel*: representative traces; middle panel: plot of average data for L5 neurons; *bottom panel*: plot of average data for L2/3 neurons). Statistically different between before and after application of HCN channel blocker ZD7288, *$P < 0.05$; #$P < 0.01$ (repeated-measures ANOVA followed by paired *t*-test; number of cells are in parentheses). Scale bar: 40 mV, 100 ms.

of mPFC neurons may help elucidate the mechanisms underlying information process as well as mPFC-dependent cognitive processes.

Another functional implication for the layer-specific variations in membrane potential is the involvement of cortical neurons in slow oscillations (<1 Hz), which are observed during quiet wakefulness or sleep and manifested by a bistability of RMP (Metherate et al. 1992; Steriade et al. 1993a, 1993b). Such slow oscillations are observed in neocortex, including mPFC, and is thought to be important for memory consolidation (Eschenko et al. 2012; Steriade et al. 1993b). Interestingly, a recent study by Beltramo and colleagues (2013) revealed that periodic activation of L5 but not L2/3 neurons resulted in almost complete entrainment of ongoing slow-frequency field potentials at the stimulation frequency (1 Hz). Furthermore, several studies indicate that the slow oscillations originate in deep layers and then spread to more superficial cortical layers (Beltramo et al. 2013; Sakata and Harris 2009; Sanchez-Vives and McCormick 2000). In addition, there is evidence showing that slow oscillation only occurs at a specific range of membrane potential in thalamic neurons and when *h*-current is present (Lüthi and McCormick 1998; McCormick

and Pape 1990). Thus, although both L2/3 and L5 neurons may receive similar incoming synaptic stimulation, L5 neurons are more likely to be excited and generate synchronized activity than L2/3 neurons. The current observations that RMP and I_h levels vary across layers suggest that L5 neurons are the source of cortical slow oscillation and critical for memory consolidation.

The mPFC has extensive reciprocal connections with other cortical or subcortical areas such as mediodorsal thalamus, and amygdala (Thomson and Bannister 2003; Verwer et al. 1996). Interestingly, the afferent inputs to the mPFC also display subregion specificity. For instance, the BLA axons preferentially target L2 over L5 within PL, whereas they preferentially target L5 within IL (Cheriyan et al. 2016; but see Bacon et al. 1996, where a different projection pattern was shown). Given the current findings that L5 neurons are more excitable than L2/3 neurons, these data suggest that the BLA inputs preferentially activate infralimbic L5 neurons over other subregions. In addition, fear conditioning and extinction not only modulate the physiological properties within mPFC but also modulate the activity of upstream and downstream neurons within neuronal circuit. Specifically, fear conditioning selectively activates BLA-PL projection neurons whereas extinction activates BLA-IL projection neurons (Senn et al. 2014). Furthermore, retrieval of a remote conditioned fear memory selectively activates the neurons within paraventricular nucleus of the thalamus, which receives synaptic projections from mPFC (Do-Monte et al. 2015). Thus, although the exact fear memory circuit is still unclear, the mPFC is at a critical position for the expression and extinction of conditioned fear.

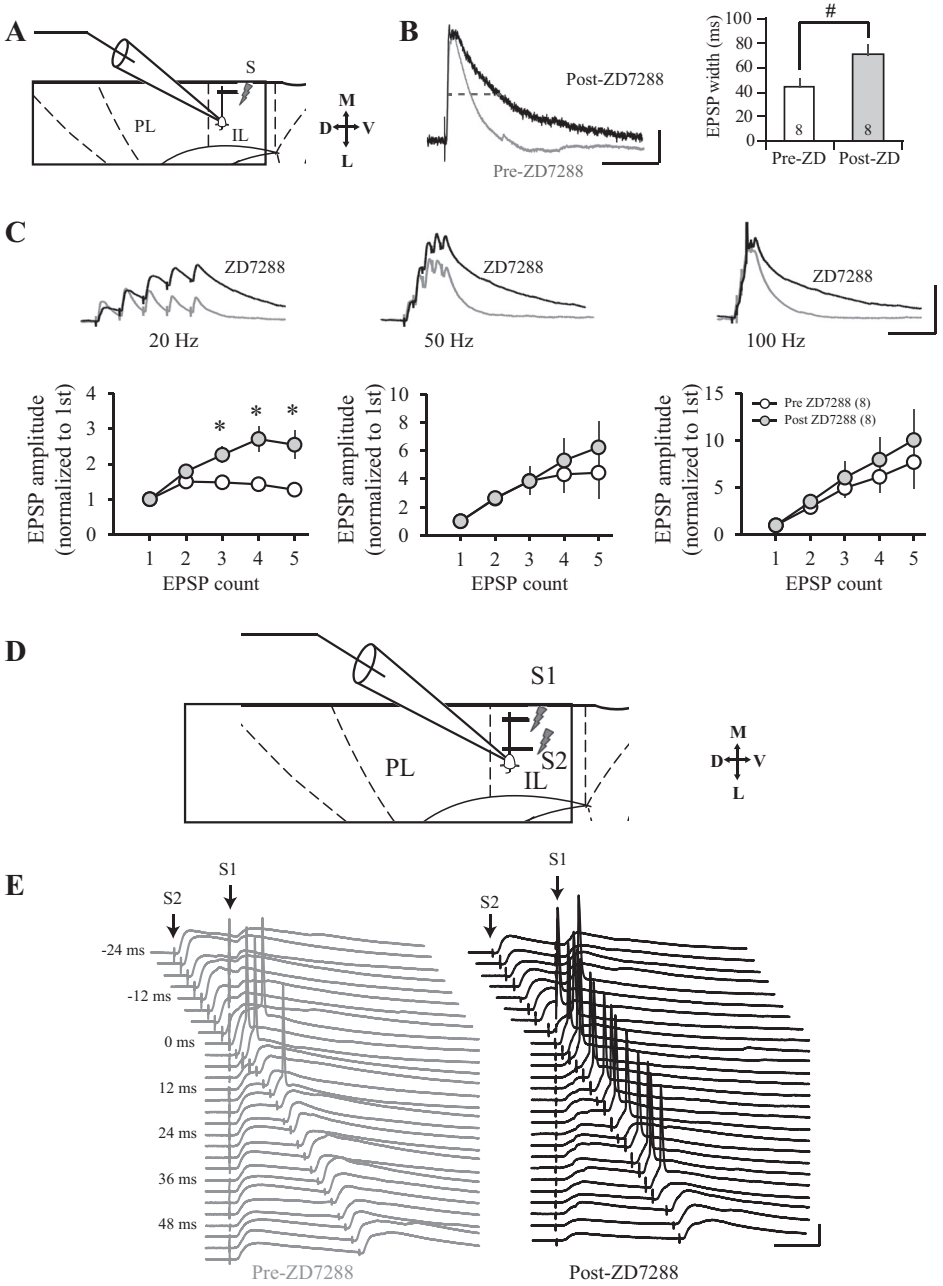

Fig. 7. Blocking I_h facilitates temporal summation and coincidence detection of mPFC- basolateral complex of amygdala (BLA) projection neurons. *A*: schematic showing the experimental setup used to study the effect of ZD7288 (ZD) on dendritic signal integration. Whole-cell recording was performed on L5 mPFC-BLA projection neurons and dendritic excitatory postsynaptic potentials (EPSPs) were evoked by stimulating L2/3 fibers using an electrode located within 100 μm of the apical dendrites. D, dorsal; L, lateral; M, medial; S, stimulating electrode; V, ventral. *B*: representative voltage traces (*left*) and summary data plot (*right;* numbers located within the bar graphs represent the number of cells in that group.) showing that blocking I_h increased the width of single EPSPs evoked by stimulating L2/3 [$t(7) = 3.8$, $P = 0.007$; paired *t*-test]. Scale bar, 5 mV, 100 ms. *C*: representative voltage traces (*top*) and summarized data plots (*bottom*; normalized EPSP amplitude to the first EPSP) showing that blocking I_h facilitated temporal summation of dendritic EPSPs, especially at lower frequencies [$F(1,12) = 9.1$, $P = 0.011$ for 20 Hz; $F(1,12) = 0.18$, $P = 0.68$ for 50 Hz; $F(1,12) = 0.35$, $P = 0.57$ for 100 Hz, respectively; repeated-measures ANOVA. Significantly different between normalized EPSP amplitude between pre- and post-ZD7288 application, $^*P < 0.05$, paired *t*-test; number of cells are in parentheses]. AP was truncated in the 100 Hz traces for clarity. Scale bar, 10 mV, 100 ms. *D*: schematic showing the experimental setup used to study the effect of ZD7288 on coincidence detection. EPSPs were evoked by stimulating L2/3 and L5 within 100 μm of the apical dendrites of the recorded neuron. *E*: bath application of ZD7288 facilitates coincidence detection. Under both control condition (*left*) and in the presence of ZD7288 (*right*), threshold stimulation intensities were adjusted to reliably evoke a spike when there was no delay between the two stimuli. The interstimulus interval (ISI) was then systematically varied by increasing the interval by 3 ms on subsequent stimulation sweeps. Compared with the pre-ZD7288 application (*left*), following application of ZD7288 (*right*), APs were more readily evoked by the two stimuli even when the ISI between them became larger. Scale bar, 20 mV, 20 ms.

IL Neurons Are More Excitable Than PL Neurons

Within L2/3, neurons obtained from IL were more excitable than those obtained from PL, as evidenced by IL neurons firing more spikes in response to current injections (Fig. 5*C*). Such differential intrinsic excitability was associated with lower AP threshold, higher input resistance, and lower $I_{threshold}$ in IL neurons than those in PL neurons. These observations are consistent with our previous report where we found that disruption of the differential excitability between IL and PL in aged animals may underlie the observed age-related extinction deficits (Kaczorowski et al. 2012). Interestingly, the current study demonstrates that such subregion-specific differences in intrinsic excitability do not exist in L5 neurons. Thus, maintaining such subregion-specific intrinsic excitability within mPFC is critical for the expression of conditioned fear memory, whereas abnormal intrinsic excitability in mPFC may lead to extinction deficits (Kaczorowski et al. 2012).

In neocortex, the pyramidal neurons within L5 provide the major cortical output to subcortical targets (Groh et al. 2010). However, these neurons are highly heterogeneous in both anatomical and physiological properties depending upon their long-range projection targets (Dembrow et al. 2010, 2015; Hattox and Nelson 2007; Larkman and Mason 1990; Mason and Larkman 1990; Xiao et al. 2009). Different types of neurons may play distinct roles during learning and memory. This was demonstrated in our recent study showing that trace fear conditioning significantly enhanced the excitability of regular spiking IL-BLA projection neurons but suppressed the excitability of PL-BLA projection neurons (Song et al. 2015). Furthermore, the increase in intrinsic excitability in IL-BLA projection neurons was associated with a reduction in AP threshold and increase in I_h, whereas the reduction of intrinsic excitability of PL-BLA projection neurons was associated with a decrease in input resistance (Song et al. 2015). Similar results have been reported in mPFC following olfactory fear conditioning. Those mPFC neurons that receive monosynaptic inputs from the BLA fired more spikes in response to conditioned odor but not to nonconditioned odor (Laviolette et al. 2005). Moreover, the conditioned odor elicited greater excitation in those IL neurons that project to the nucleus accumbens than in those mPFC neurons that project to the contralateral mPFC (McGinty and Grace 2008). In addition, a recent study suggests that activation of IL neurons suppresses PL neuronal activity (Ji and Neugebauer 2012), which may be an important mechanism underlying the opposite roles of IL and PL in fear memory acquisition. Thus, the role of mPFC during information processing is determined not only by subregion-specific variations in neuronal intrinsic excitability, but also by local and remote synaptic connections.

Table 5. *Correlations between somata location (somatic depth) and electrophysiological properties*

	IL			PL		
Measurements	*n*	*r*	*P*	*n*	*r*	*P*
RMP	53	0.52	0.001†	32	0.72	0.001†
R_N	53	0.12	0.41	32	0.27	0.130
Sag ratio	48	0.40	0.005†	29	0.55	0.002†
$I_{threshold}$	47	−0.10	0.52	30	−0.39	0.032‡
postburst mAHP	50	0.23	0.11	32	0.51	0.003†
postburst sAHP	50	0.11	0.44	32	0.42	0.017*
No. of spikes	47	0.13	0.37	31	0.46	0.009†

RMP, resting membrane potential; R_N, input resistance; $I_{threshold}$, threshold current required to elicit one action potential. No. of spikes was counted from the spikes evoked by a 300-pA current injection. *Significant correlation for Pearson's correlation coefficient, $P < 0.05$; †Significant correlation for Pearson's correlation coefficient, $P < 0.01$; ‡Significant correlation for Spearman's correlation coefficient: $P < 0.05$.

I_h Modulates Intrinsic and Synaptic Properties of Layer 5 mPFC Neurons

The strong effect of ZD7288 on the membrane properties of L5 mPFC pyramidal neurons suggests that I_h is critical for basic neuronal functions. Our data are consistent with previous reports showing that HCN channels are critical for maintaining membrane potential, regulating input resistance, as well as influencing the duration of synaptic EPSPs and signal integration (Dembrow et al. 2010, 2015; Magee 1998, 1999). Interestingly, we also observed that HCN channels are involved in shaping AP waveform of IL-BLA projection neurons, as evidenced by an increase in spike width following the blockade of I_h (see Fig. 6*B*). This is in line with the observation that blocking I_h with ZD7288 significantly increased spike width in rat inner hair cell afferent synapses (Yi et al. 2010).

Our observed contributions for I_h in the neurophysiological properties of L5 mPFC neurons are consistent with previous reports in neurons from other regions such as hippocampal CA1 and the superior colliculus (Endo et al. 2008; Nolan et al. 2004; Pavlov et al. 2011; Vaidya and Johnston 2013). I_h prevents the integration of low-frequency inputs whereas it allows the passage of high-frequency signals. Such a filter effect may manifest a mechanism of I_h through which mPFC-BLA neurons can selectively respond to salient environment stimuli (e.g., high-frequency signals) whereas other stimuli (e.g., low-frequency signals) are filtered out. Our recent observation that I_h was enhanced in regular spiking IL-BLA projection neurons following trace fear conditioning suggests that I_h is involved in the acquisition and recall of conditioned fear in mPFC neurons (Song et al. 2015). Interestingly, in that study we also found an increase in intrinsic excitability in IL-BLA projection neurons, which seems contradictory to the current finding that pharmacological blockade of I_h enhances intrinsic excitability. However, in our previous study (Song et al. 2015), the learning-induced enhancement of intrinsic excitability was associated with an increased I_h and a decrease in spike threshold without any significant changes in input resistance. In addition, because the equilibrium potential of HCN channels is about −30 mV (Mayer and Westbrook 1983) and is higher than the spike threshold, HCN channel currents depolarize the membrane in response to current injection. Furthermore, the inhibitory effect of HCN channels is more prominent for dendritic EPSP because the channels are highly distributed in distal dendrites (Magee 1998). Thus, although HCN channels inhibits synaptic EPSP, the inhibitory effect is masked by the depolarization of membrane potential when depolarizing current was injected to soma (Kase and Imoto 2012).

Layer- and Subregion-Specific Electrophysiological Properties of mPFC Neurons

In the current study, we found that the differential expression of HCN channels between L2/3 and L5 partially accounts

for the layer-specific properties, whereas the different input resistance between IL and PL partially accounts for the subregion-specific membrane properties. It has been well established that HCN channels contribute to RMP, R_N, and membrane time constant in cortical neurons (Lüthi and McCormick 1998; Magee 1998; Pape 1996). Our observation that L2/3 neurons were not significantly changed by HCN channel blockers is consistent with previous data that HCN channels are not detectable in L2/3 (Lörincz et al. 2002). The different input resistance between IL and PL neurons is also consistent with our previous study in L2/3 neurons (Kaczorowski et al. 2012).

That the complexity of the basal but not apical dendrites dramatically affects the intrinsic excitability is particularly interesting because it has been determined that the basal dendrites are the major target for synaptic inputs (Larkman 1991) but the computational function of basal dendrites is still poorly understood. In addition to distinct morphological feature between these two types of dendrites, ion channels are also expressed differently and therefore have distinct electrophysiological properties. For example, the expression of HCN channels is very low in basal dendrites but much higher in distal apical dendrites, where they dramatically reduce the excitability (Breton and Stuart 2009; Larkum et al. 2009; Magee 1998; Nevian et al. 2007; Nikmaram et al. 1997). In addition, the sodium spikes evoked in basal dendrites are fast and display little attenuation whereas the sodium spikes triggered in apical dendrites have a significant attenuation (Kim et al. 2011), suggesting different expression of ion channels between basal and apical dendrites. However, it is less clear how the complexity of the basal dendrites contributes to the intrinsic excitability, which may be a potential interest for future studies.

In addition to intrinsic properties, the efferent and afferent synaptic connections are also different between neurons within IL and PL. The inputs to mPFC come primarily from limbic structures, including the hippocampus, the agranular insular cortex, and the BLA (Hoover and Vertes 2007). However, the pattern of inputs is layer and subregion specific such that each subregion receives a unique set of afferent projections (Hoover and Vertes 2007). For example, BLA innervates both L2 and L5 within mPFC, but the density of BLA axons is higher in infralimbic L5 and prelimbic L2 (Cheriyan et al. 2016). Considering the subregion-specific excitability of mPFC neurons, it is likely that BLA activity preferentially activates infralimbic L5 neurons. In addition, the local mPFC microcircuits are also layer specific. Layer 2/3 pyramidal neurons selectively innervate and excite pyramidal neurons in L5, but direct synaptic connections from L5 to L2/3 pyramidal neurons are rare (Otsuka and Kawaguchi 2008; Thomson and Bannister 1998; Thomson et al. 2002). Thus, both L2/3 and L5 neurons receive inputs from limbic structures, but L5 neurons also integrate information coming from L2/3 neurons.

Implications for Modulation of Emotional Learning

The current study demonstrated that in mPFC neurons synaptic integration is greatly affected by modulation of HCN channels (see Fig. 7). Within the brain, multiple neurotransmitters, including both dopamine (Gamo et al. 2015) and norepinephrine (Carr et al. 2007; Shirasaka et al. 2007) are capable of modulating HCN channels and thus influencing information processing. For example, voltage-clamp analyses in rat prefrontal neurons indicate that activation of α2-adrenergic receptors (α2ARs) significantly reduces I_h (Carr et al. 2007). Multiple lines of evidence have also shown that stress hormones are released and the noradrenergic system is activated during emotional learning (e.g., McGaugh and Roozendaal 2009), suggesting one mechanism by which modulation of HCN channels occurs during emotional learning. Interestingly, blocking HCN channels through activating postsynaptic α2ARs are found to facilitate spatial learning and working memory (Arnsten and Jin 2014) but not fear conditioning (Jin et al. 2007), whereas administration of adrenergic drugs or hormones that indirectly activate HCN channels through blocking α2ARs and activate β receptors (Xing et al. 2016) has been shown to enhance associative fear memory (Soeter and Kindt 2011) or emotionally arousing information (Cahill and Alkire 2003; Southwick et al. 2002) in human subjects. Thus, the modulation of HCN channels might be task specific and may be increased following some types of learning such as trace eyeblink conditioning (Moyer et al. 1996) and trace fear conditioning (Song et al. 2015). These studies and our current data also suggest that maintaining physiological level of HCN channels within cortical neurons is critical for cognitive function whereas the advantage of layer-specific distribution of these channels still needs to be explored.

Conclusions

The current study demonstrates that the mPFC neurons are highly heterogeneous in a layer- and subregion-specific manner. L2/3 neurons are significantly hyperpolarized and less excitable than L5 neurons. IL neurons are more excitable than PL neurons within L2/3 but not L5. Furthermore, within mPFC the L2/3 neurons have less *h*-current than that of L5 neurons. Such layer-specific expression of HCN channels may underlie the laminar differences in neuronal intrinsic properties and signal integration. These data suggest that the layer- and subregion-specific properties may underlie distinct functional roles of IL and PL in fear conditioning and extinction.

ACKNOWLEDGMENTS

Present address for C. Song: Department of Neuroscience, The Scripps Research Institute, Jupiter, FL 33458.

GRANTS

This study was supported by a Research Growth Initiative from the University of Wisconsin-Milwaukee (J. R. Moyer) and NIA grant R03-AG042814 (J. R. Moyer).

DISCLOSURES

No conflicts of interest, financial or otherwise, are declared by the authors.

AUTHOR CONTRIBUTIONS

C.S. and J.R.M. conceived and designed research; C.S. performed experiments; C.S. analyzed data; C.S. and J.R.M. interpreted results of experiments; C.S. prepared figures; C.S. drafted manuscript; C.S. and J.R.M. edited and revised manuscript; C.S. and J.R.M. approved final version of manuscript.

REFERENCES

Aou S, Woody CD, Birt D. Increases in excitability of neurons of the motor cortex of cats after rapid acquisition of eye blink conditioning. *J Neurosci* 12: 560–569, 1992.

Arnsten AF, Jin LE. Molecular influences on working memory circuits in dorsolateral prefrontal cortex. *Prog Mol Biol Transl Sci* 122: 211–231, 2014. doi:10.1016/B978-0-12-420170-5.00008-8.

Arruda-Carvalho M, Clem RL. Pathway-selective adjustment of prefrontal-amygdala transmission during fear encoding. *J Neurosci* 34: 15601–15609, 2014. doi:10.1523/JNEUROSCI.2664-14.2014.

Bacon SJ, Headlam AJ, Gabbott PL, Smith AD. Amygdala input to medial prefrontal cortex (mPFC) in the rat: a light and electron microscope study. *Brain Res* 720: 211–219, 1996. doi:10.1016/0006-8993(96)00155-2.

Becker K, Eder M, Ranft A, von Meyer L, Zieglgänsberger W, Kochs E, Dodt HU. Low dose isoflurane exerts opposing effects on neuronal network excitability in neocortex and hippocampus. *PLoS One* 7: e39346, 2012. doi:10.1371/journal.pone.0039346.

Beltramo R, D'Urso G, Dal Maschio M, Farisello P, Bovetti S, Clovis Y, Lassi G, Tucci V, De Pietri Tonelli D, Fellin T. Layer-specific excitatory circuits differentially control recurrent network dynamics in the neocortex. *Nat Neurosci* 16: 227–234, 2013. doi:10.1038/nn.3306.

Boudewijns ZS, Groen MR, Lodder B, McMaster MT, Kalogreades L, de Haan R, Narayanan RT, Meredith RM, Mansvelder HD, de Kock CP. Layer-specific high-frequency action potential spiking in the prefrontal cortex of awake rats. *Front Cell Neurosci* 7: 99, 2013. doi:10.3389/fncel.2013.00099.

Breton JD, Stuart GJ. Loss of sensory input increases the intrinsic excitability of layer 5 pyramidal neurons in rat barrel cortex. *J Physiol* 587: 5107–5119, 2009. doi:10.1113/jphysiol.2009.180943.

Burgos-Robles A, Vidal-Gonzalez I, Quirk GJ. Sustained conditioned responses in prelimbic prefrontal neurons are correlated with fear expression and extinction failure. *J Neurosci* 29: 8474–8482, 2009. doi:10.1523/JNEUROSCI.0378-09.2009.

Burgos-Robles A, Vidal-Gonzalez I, Santini E, Quirk GJ. Consolidation of fear extinction requires NMDA receptor-dependent bursting in the ventromedial prefrontal cortex. *Neuron* 53: 871–880, 2007. doi:10.1016/j.neuron.2007.02.021.

Cahill L, Alkire MT. Epinephrine enhancement of human memory consolidation: interaction with arousal at encoding. *Neurobiol Learn Mem* 79: 194–198, 2003. doi:10.1016/S1074-7427(02)00036-9.

Carr DB, Andrews GD, Glen WB, Lavin A. alpha2-Noradrenergic receptors activation enhances excitability and synaptic integration in rat prefrontal cortex pyramidal neurons via inhibition of HCN currents. *J Physiol* 584: 437–450, 2007. doi:10.1113/jphysiol.2007.141671.

Chang CH, Maren S. Medial prefrontal cortex activation facilitates re-extinction of fear in rats. *Learn Mem* 18: 221–225, 2011. doi:10.1101/lm.2070111.

Cheriyan J, Kaushik MK, Ferreira AN, Sheets PL. Specific targeting of the basolateral amygdala to projectionally defined pyramidal neurons in prelimbic and infralimbic cortex. *eNeuro* 3: 3, 2016. doi:10.1523/ENEURO.0002-16.2016.

Connors BW, Gutnick MJ, Prince DA. Electrophysiological properties of neocortical neurons in vitro. *J Neurophysiol* 48: 1302–1320, 1982.

Daoudal G, Debanne D. Long-term plasticity of intrinsic excitability: learning rules and mechanisms. *Learn Mem* 10: 456–465, 2003. doi:10.1101/lm.64103.

Dembrow NC, Chitwood RA, Johnston D. Projection-specific neuromodulation of medial prefrontal cortex neurons. *J Neurosci* 30: 16922–16937, 2010. doi:10.1523/JNEUROSCI.3644-10.2010.

Dembrow NC, Zemelman BV, Johnston D. Temporal dynamics of L5 dendrites in medial prefrontal cortex regulate integration versus coincidence detection of afferent inputs. *J Neurosci* 35: 4501–4514, 2015. doi:10.1523/JNEUROSCI.4673-14.2015.

Do-Monte FH, Quiñones-Laracuente K, Quirk GJ. A temporal shift in the circuits mediating retrieval of fear memory. *Nature* 519: 460–463, 2015. doi:10.1038/nature14030.

Eckle VS, Digruccio MR, Uebele VN, Renger JJ, Todorovic SM. Inhibition of T-type calcium current in rat thalamocortical neurons by isoflurane. *Neuropharmacology* 63: 266–273, 2012. doi:10.1016/j.neuropharm.2012.03.018.

Endo T, Tarusawa E, Notomi T, Kaneda K, Hirabayashi M, Shigemoto R, Isa T. Dendritic Ih ensures high-fidelity dendritic spike responses of motion-sensitive neurons in rat superior colliculus. *J Neurophysiol* 99: 2066–2076, 2008. doi:10.1152/jn.00556.2007.

Eschenko O, Magri C, Panzeri S, Sara SJ. Noradrenergic neurons of the locus coeruleus are phase locked to cortical up-down states during sleep. *Cereb Cortex* 22: 426–435, 2012. doi:10.1093/cercor/bhr121.

Fan Y, Fricker D, Brager DH, Chen X, Lu HC, Chitwood RA, Johnston D. Activity-dependent decrease of excitability in rat hippocampal neurons through increases in I(h). *Nat Neurosci* 8: 1542–1551, 2005. doi:10.1038/nn1568.

Gabbott PL, Bacon SJ. Local circuit neurons in the medial prefrontal cortex (areas 24a,b,c, 25 and 32) in the monkey: I. Cell morphology and morphometrics. *J Comp Neurol* 364: 567–608, 1996. doi:10.1002/(SICI)1096-9861(19960122)364:4<567::AID-CNE1>3.0.CO;2-1.

Gaillard F, Sauve Y. Fetal tissue allografts in the central visual system of rodents. In *Webvision: The Organization of the Retina and Visual System*, edited by Kolb H, Fernandez E, Nelson R. Salt Lake City, UT: University of Utah Health Sciences Center, 1995.

Gamo NJ, Lur G, Higley MJ, Wang M, Paspalas CD, Vijayraghavan S, Yang Y, Ramos BP, Peng K, Kata A, Boven L, Lin F, Roman L, Lee D, Arnsten AF. Stress impairs prefrontal cortical function via D_1 dopamine receptor interactions with hyperpolarization-activated cyclic nucleotide-gated channels. *Biol Psychiatry* 78: 860–870, 2015. doi:10.1016/j.biopsych.2015.01.009.

Garcia R, Vouimba RM, Baudry M, Thompson RF. The amygdala modulates prefrontal cortex activity relative to conditioned fear. *Nature* 402: 294–296, 1999. doi:10.1038/46286.

Groh A, Meyer HS, Schmidt EF, Heintz N, Sakmann B, Krieger P. Cell-type specific properties of pyramidal neurons in neocortex underlying a layout that is modifiable depending on the cortical area. *Cereb Cortex* 20: 826–836, 2010. doi:10.1093/cercor/bhp152.

Hattox AM, Nelson SB. Layer V neurons in mouse cortex projecting to different targets have distinct physiological properties. *J Neurophysiol* 98: 3330–3340, 2007. doi:10.1152/jn.00397.2007.

Hayton SJ, Olmstead MC, Dumont ÉC. Shift in the intrinsic excitability of medial prefrontal cortex neurons following training in impulse control and cued-responding tasks. *PLoS One* 6: e23885, 2011. doi:10.1371/journal.pone.0023885.

Heidbreder CA, Groenewegen HJ. The medial prefrontal cortex in the rat: evidence for a dorso-ventral distinction based upon functional and anatomical characteristics. *Neurosci Biobehav Rev* 27: 555–579, 2003. doi:10.1016/j.neubiorev.2003.09.003.

Hoover WB, Vertes RP. Anatomical analysis of afferent projections to the medial prefrontal cortex in the rat. *Brain Struct Funct* 212: 149–179, 2007. doi:10.1007/s00429-007-0150-4.

Ji G, Neugebauer V. Modulation of medial prefrontal cortical activity using in vivo recordings and optogenetics. *Mol Brain* 5: 36, 2012. doi:10.1186/1756-6606-5-36.

Jin XC, Ma CL, Li BM. The α(2A)-adrenoceptor agonist guanfacine improves spatial learning but not fear conditioning in rats. *Sheng Li Xue Bao* 59: 739–744, 2007.

Joksovic PM, Todorovic SM. Isoflurane modulates neuronal excitability of the nucleus reticularis thalami in vitro. *Ann N Y Acad Sci* 1199: 36–42, 2010. doi:10.1111/j.1749-6632.2009.05172.x.

Kaczorowski CC, Davis SJ, Moyer JR Jr. Aging redistributes medial prefrontal neuronal excitability and impedes extinction of trace fear conditioning. *Neurobiol Aging* 33: 1744–1757, 2012. doi:10.1016/j.neurobiolaging.2011.03.020.

Kase D, Imoto K. The role of HCN channels on membrane excitability in the nervous system. *J Signal Transduct* 2012: 619747, 2012. doi:10.1155/2012/619747.

Kim JJ, Jung MW. Neural circuits and mechanisms involved in Pavlovian fear conditioning: a critical review. *Neurosci Biobehav Rev* 30: 188–202, 2006. doi:10.1016/j.neubiorev.2005.06.005.

Kim MJ, Loucks RA, Palmer AL, Brown AC, Solomon KM, Marchante AN, Whalen PJ. The structural and functional connectivity of the amygdala: from normal emotion to pathological anxiety. *Behav Brain Res* 223: 403–410, 2011. doi:10.1016/j.bbr.2011.04.025.

Kwapis JL, Jarome TJ, Helmstetter FJ. The role of the medial prefrontal cortex in trace fear extinction. *Learn Mem* 22: 39–46, 2015. doi:10.1101/lm.036517.114.

Larkman A, Mason A. Correlations between morphology and electrophysiology of pyramidal neurons in slices of rat visual cortex. I. Establishment of cell classes. *J Neurosci* 10: 1407–1414, 1990.

Larkman AU. Dendritic morphology of pyramidal neurones of the visual cortex of the rat: III. Spine distributions. *J Comp Neurol* 306: 332–343, 1991. doi:10.1002/cne.903060209.

Larkum ME, Nevian T, Sandler M, Polsky A, Schiller J. Synaptic integration in tuft dendrites of layer 5 pyramidal neurons: a new unifying principle. *Science* 325: 756–760, 2009. doi:10.1126/science.1171958.

Laviolette SR, Lipski WJ, Grace AA. A subpopulation of neurons in the medial prefrontal cortex encodes emotional learning with burst and frequency codes through a dopamine D4 receptor-dependent basolateral amygdala input. *J Neurosci* 25: 6066–6075, 2005. doi:10.1523/JNEUROSCI.1168-05.2005.

Lörincz A, Notomi T, Tamás G, Shigemoto R, Nusser Z. Polarized and compartment-dependent distribution of HCN1 in pyramidal cell dendrites. *Nat Neurosci* 5: 1185–1193, 2002. doi:10.1038/nn962.

Lüthi A, McCormick DA. H-current: properties of a neuronal and network pacemaker. *Neuron* 21: 9–12, 1998. doi:10.1016/S0896-6273(00)80509-7.

Magee JC. Dendritic hyperpolarization-activated currents modify the integrative properties of hippocampal CA1 pyramidal neurons. *J Neurosci* 18: 7613–7624, 1998.

Magee JC. Dendritic Ih normalizes temporal summation in hippocampal CA1 neurons. *Nat Neurosci* 2: 848, 1999. doi:10.1038/12229.

Mason A, Larkman A. Correlations between morphology and electrophysiology of pyramidal neurons in slices of rat visual cortex. II. Electrophysiology. *J Neurosci* 10: 1415–1428, 1990.

Mayer ML, Westbrook GL. A voltage-clamp analysis of inward (anomalous) rectification in mouse spinal sensory ganglion neurones. *J Physiol* 340: 19–45, 1983. doi:10.1113/jphysiol.1983.sp014747.

McCormick DA, Pape HC. Properties of a hyperpolarization-activated cation current and its role in rhythmic oscillation in thalamic relay neurones. *J Physiol* 431: 291–318, 1990. doi:10.1113/jphysiol.1990.sp018331.

McGaugh JL, Roozendaal B. Drug enhancement of memory consolidation: historical perspective and neurobiological implications. *Psychopharmacology (Berl)* 202: 3–14, 2009. doi:10.1007/s00213-008-1285-6.

McGinty VB, Grace AA. Selective activation of medial prefrontal-to-accumbens projection neurons by amygdala stimulation and Pavlovian conditioned stimuli. *Cereb Cortex* 18: 1961–1972, 2008. doi:10.1093/cercor/bhm223.

Medini P. Layer- and cell-type-specific subthreshold and suprathreshold effects of long-term monocular deprivation in rat visual cortex. *J Neurosci* 31: 17134–17148, 2011. doi:10.1523/JNEUROSCI.2951-11.2011.

Metherate R, Cox CL, Ashe JH. Cellular bases of neocortical activation: modulation of neural oscillations by the nucleus basalis and endogenous acetylcholine. *J Neurosci* 12: 4701–4711, 1992.

Milad MR, Quirk GJ. Neurons in medial prefrontal cortex signal memory for fear extinction. *Nature* 420: 70–74, 2002. doi:10.1038/nature01138.

Milad MR, Vidal-Gonzalez I, Quirk GJ. Electrical stimulation of medial prefrontal cortex reduces conditioned fear in a temporally specific manner. *Behav Neurosci* 118: 389–394, 2004. doi:10.1037/0735-7044.118.2.389.

Morgan MA, LeDoux JE. Differential contribution of dorsal and ventral medial prefrontal cortex to the acquisition and extinction of conditioned fear in rats. *Behav Neurosci* 109: 681–688, 1995. doi:10.1037/0735-7044.109.4.681.

Moyer JR Jr, Brown TH. Visually-guided patch-clamp recordings in brain slices. In: *Advanced Techniques for Patch-Clamp Analysis*, edited by Walz W. Totowa, NJ: Humana, 2007, p. 169–227. doi:10.1007/978-1-59745-492-6_6.

Moyer JR Jr, McNay EC, Brown TH. Three classes of pyramidal neurons in layer V of rat perirhinal cortex. *Hippocampus* 12: 218–234, 2002. doi:10.1002/hipo.1110.

Moyer JR Jr, Thompson LT, Disterhoft JF. Trace eyeblink conditioning increases CA1 excitability in a transient and learning-specific manner. *J Neurosci* 16: 5536–5546, 1996.

Nevian T, Larkum ME, Polsky A, Schiller J. Properties of basal dendrites of layer 5 pyramidal neurons: a direct patch-clamp recording study. *Nat Neurosci* 10: 206–214, 2007. doi:10.1038/nn1826.

Nikmaram MR, Boyett MR, Kodama I, Suzuki R, Honjo H. Variation in effects of Cs+, UL-FS-49, and ZD-7288 within sinoatrial node. *Am J Physiol Heart Circ Physiol* 272: H2782–H2792, 1997.

Nolan MF, Malleret G, Dudman JT, Buhl DL, Santoro B, Gibbs E, Vronskaya S, Buzsáki G, Siegelbaum SA, Kandel ER, Morozov A. A behavioral role for dendritic integration: HCN1 channels constrain spatial memory and plasticity at inputs to distal dendrites of CA1 pyramidal neurons. *Cell* 119: 719–732, 2004. doi:10.1016/j.cell.2004.11.020.

O'Leary T, van Rossum MC, Wyllie DJ. Homeostasis of intrinsic excitability in hippocampal neurones: dynamics and mechanism of the response to chronic depolarization. *J Physiol* 588: 157–170, 2010. doi:10.1113/jphysiol.2009.181024.

Otsuka T, Kawaguchi Y. Firing-pattern-dependent specificity of cortical excitatory feed-forward subnetworks. *J Neurosci* 28: 11186–11195, 2008. doi:10.1523/JNEUROSCI.1921-08.2008.

Pape HC. Queer current and pacemaker: the hyperpolarization-activated cation current in neurons. *Annu Rev Physiol* 58: 299–327, 1996. doi:10.1146/annurev.ph.58.030196.001503.

Pavlov I, Scimemi A, Savtchenko L, Kullmann DM, Walker MC. I(h)-mediated depolarization enhances the temporal precision of neuronal integration. *Nat Commun* 2: 199, 2011. doi:10.1038/ncomms1202.

Paxinos G, Watson C. *The Rat Brain in Stereotaxic Coordinates*. San Diego: Academic, 1998.

Perez-Cruz C, Müller-Keuker JI, Heilbronner U, Fuchs E, Flügge G. Morphology of pyramidal neurons in the rat prefrontal cortex: lateralized dendritic remodeling by chronic stress. *Neural Plast* 2007: 46276, 2007. doi:10.1155/2007/46276.

Sakata S, Harris KD. Laminar structure of spontaneous and sensory-evoked population activity in auditory cortex. *Neuron* 64: 404–418, 2009. doi:10.1016/j.neuron.2009.09.020.

Sanchez-Vives MV, McCormick DA. Cellular and network mechanisms of rhythmic recurrent activity in neocortex. *Nat Neurosci* 3: 1027–1034, 2000. doi:10.1038/79848.

Santini E, Quirk GJ, Porter JT. Fear conditioning and extinction differentially modify the intrinsic excitability of infralimbic neurons. *J Neurosci* 28: 4028–4036, 2008. doi:10.1523/JNEUROSCI.2623-07.2008.

Senn V, Wolff SB, Herry C, Grenier F, Ehrlich I, Gründemann J, Fadok JP, Müller C, Letzkus JJ, Lüthi A. Long-range connectivity defines behavioral specificity of amygdala neurons. *Neuron* 81: 428–437, 2014. doi:10.1016/j.neuron.2013.11.006.

Sepulveda-Orengo MT, Lopez AV, Soler-Cedeño O, Porter JT. Fear extinction induces mGluR5-mediated synaptic and intrinsic plasticity in infralimbic neurons. *J Neurosci* 33: 7184–7193, 2013. doi:10.1523/JNEUROSCI.5198-12.2013.

Shirasaka T, Kannan H, Takasaki M. Activation of a G protein-coupled inwardly rectifying K+ current and suppression of Ih contribute to dexmedetomidine-induced inhibition of rat hypothalamic paraventricular nucleus neurons. *Anesthesiology* 107: 605–615, 2007. doi:10.1097/01.anes.0000281916.65365.4e.

Soeter M, Kindt M. Noradrenergic enhancement of associative fear memory in humans. *Neurobiol Learn Mem* 96: 263–271, 2011. doi:10.1016/j.nlm.2011.05.003.

Soler-Cedeño O, Cruz E, Criado-Marrero M, Porter JT. Contextual fear conditioning depresses infralimbic excitability. *Neurobiol Learn Mem* 130: 77–82, 2016. doi:10.1016/j.nlm.2016.01.015.

Song C, Detert JA, Sehgal M, Moyer JR Jr. Trace fear conditioning enhances synaptic and intrinsic plasticity in rat hippocampus. *J Neurophysiol* 107: 3397–3408, 2012. doi:10.1152/jn.00692.2011.

Song C, Ehlers VL, Moyer JR Jr. Trace fear conditioning differentially modulates intrinsic excitability of medial prefrontal cortex-basolateral complex of amygdala projection neurons in infralimbic and prelimbic cortices. *J Neurosci* 35: 13511–13524, 2015. doi:10.1523/JNEUROSCI.2329-15.2015.

Southwick SM, Davis M, Horner B, Cahill L, Morgan CA III, Gold PE, Bremner JD, Charney DC. Relationship of enhanced norepinephrine activity during memory consolidation to enhanced long-term memory in humans. *Am J Psychiatry* 159: 1420–1422, 2002. doi:10.1176/appi.ajp.159.8.1420.

Steriade M, Contreras D, Curró Dossi R, Nuñez A. The slow (<1 Hz) oscillation in reticular thalamic and thalamocortical neurons: scenario of sleep rhythm generation in interacting thalamic and neocortical networks. *J Neurosci* 13: 3284–3299, 1993a.

Steriade M, Nuñez A, Amzica F. A novel slow (<1 Hz) oscillation of neocortical neurons in vivo: depolarizing and hyperpolarizing components. *J Neurosci* 13: 3252–3265, 1993b.

Thomson AM, Bannister AP. Postsynaptic pyramidal target selection by descending layer III pyramidal axons: dual intracellular recordings and biocytin filling in slices of rat neocortex. *Neuroscience* 84: 669–683, 1998. doi:10.1016/S0306-4522(97)00557-5.

Thomson AM, Bannister AP. Interlaminar connections in the neocortex. *Cereb Cortex* 13: 5–14, 2003. doi:10.1093/cercor/13.1.5.

Thomson AM, West DC, Wang Y, Bannister AP. Synaptic connections and small circuits involving excitatory and inhibitory neurons in layers 2-5 of adult rat and cat neocortex: triple intracellular recordings and biocytin labelling in vitro. *Cereb Cortex* 12: 936–953, 2002. doi:10.1093/cercor/12.9.936.

Vaidya SP, Johnston D. Temporal synchrony and gamma-to-theta power conversion in the dendrites of CA1 pyramidal neurons. *Nat Neurosci* 16: 1812–1820, 2013. doi:10.1038/nn.3562.

Varela JA, Wang J, Christianson JP, Maier SF, Cooper DC. Control over stress, but not stress per se increases prefrontal cortical pyramidal neuron excitability. *J Neurosci* 32: 12848–12853, 2012. doi:10.1523/JNEUROSCI.2669-12.2012.

Verwer RW, Van Vulpen EH, Van Uum JF. Postnatal development of amygdaloid projections to the prefrontal cortex in the rat studied with retrograde and anterograde tracers. *J Comp Neurol* 376: 75–96, 1996. doi:10.1002/(SICI)1096-9861(19961202)376:1<75::AID-CNE5>3.0.CO;2-L.

Vidal-Gonzalez I, Vidal-Gonzalez B, Rauch SL, Quirk GJ. Microstimulation reveals opposing influences of prelimbic and infralimbic cortex on the expression of conditioned fear. *Learn Mem* 13: 728–733, 2006. doi:10.1101/lm.306106.

Xiao D, Zikopoulos B, Barbas H. Laminar and modular organization of prefrontal projections to multiple thalamic nuclei. *Neuroscience* 161: 1067–1081, 2009. doi:10.1016/j.neuroscience.2009.04.034.

Xing B, Li YC, Gao WJ. Norepinephrine versus dopamine and their interaction in modulating synaptic function in the prefrontal cortex. *Brain Res* 1641: 217–233, 2016. doi:10.1016/j.brainres.2016.01.005.

Yi E, Roux I, Glowatzki E. Dendritic HCN channels shape excitatory postsynaptic potentials at the inner hair cell afferent synapse in the mammalian cochlea. *J Neurophysiol* 103: 2532–2543, 2010. doi:10.1152/jn.00506.2009.